Materials Research. 2020; 23(6): e20200337
DOI: https://doi.org/10.1590/1980-5373-MR-2020-0337

Effect of Cobalt Doping and Milling Time on Microstructure and Vickers Microhardness of the Spark Plasma Sintered (67-x)Ti-xCo-22Si-11B (x = 2 and 6 at-%) Alloys

Nelson Damásio Ferreira[a], Ricardo Mendes Leal Neto[b], Marcello Filgueira[c], Manuel Fellipe Rodrigues Pais Alves[d], Claudinei dos Santos[e], Alfeu Saraiva Ramos[a]*

[a]Universidade Federal de Alfenas, Instituto de Ciência e Tecnologia, Rodovia José Aurélio Vilela, 11999, 37715-400, Poços de Caldas, MG, Brasil
[b]Instituto de Pesquisas Energéticas e Nucleares. Av. Prof. Lineu Prestes, 2242, Cidade Universitária, Butantã, 05508-000, São Paulo, SP, Brasil
[c]Universidade Estadual do Norte Fluminense Darcy Ribeiro, Avenida Alberto Lamengo, 200, Parque Califórnia, 28013-602, Campos de Goytacazes, RJ, Brasil
[d]Escola de Engenharia de Lorena, Universidade de São Paulo, Polo Urbo Industrial, Gleba AI-6, 12602-810, Lorena, SP, Brasil
[e]Universidade do Estado do Rio de Janeiro, Faculdade de Tecnologia de Resende, Rodovia Presidente Dutra km 298, Polo Industrial de Resende, 27537-000, Resende, RJ, Brasil

Received: July 25, 2020; Revised: October 16, 2020; Accepted: November 2, 2020

Ti-6Al-4V and TiAl-based alloys are widely used for fabricating the implantable orthopedic devices and automotive components, respectively. Ti_6Si_2B-based alloys are attractive for use in orthopedic components because their higher hardness, superior biocompatibility and corrosion resistance in simulated body fluid than Ti and Ti-6Al-4V alloy. Limited information on Ti_6Si_2B stability in Co-dopped 67Ti-22Si-11B alloys are available in literature. This work presents the effect of cobalt doping and milling time on microstructure and Vickers microhardness of 65Ti-2Co-22Si-11B and 61Ti-6Co-22Si-11B (at-%) alloys produced by spark plasma sintering at 1100 °C for 12min using 20MPa. Samples were characterized by X ray diffraction, scanning electron microscopy, energy dispersive spectrometry, laser particle size analysis, and Vickers microhardness. Sintered alloys with 2 and 6at-%Co indicated the major presence of Ti_6Si_2B and Ti_5Si_3 dissolving up to 2.7 and 4.2 at-%Co, respectively, besides the minor precipitates of $CoTi_2$ (4.4-16.7at-%Si) and CoTi (4.6-4.7at-%Si). Vickers microhardness of the sintered 65Ti-2Co-22Si-11B and 61Ti-6Co-22Si-11B alloys were in the range of 950-1050 and 1050-1150HV, respectively. Although the increase from 2 to 6at-%Co has reduced the Ti_6Si_2B stability, the Co-rich phases increased their hardness values up to 1150HV (11.3GPa), which are superior than those of commercial Ti alloys used for joint orthopedic components and automotive rotating parts.

Keywords: *titanium alloys, cobalt, implants, automotive, sintering.*

1. Introduction

Ti_6Si_2B-based alloys with high hardness, corrosion resistance, and good biocompatibility and bone integration characteristics are potentially attractive for fabricating of articular orthopedic components[1,2]. Moreover, these high hardness values are also desirable for rotating components used in automotive applications[3]. Nonetheless, the use of alloying and its effect on phase transformations during processing and specific mechanical properties are important. Previous studies on phase transformations in mechanical alloyed (67-x)Ti-xMe-22Si-11B ($x \leq 6$ at-%) powders containing the Sn[4] or Zr[5] addition lower than 2 and 6 at-% can produce microstructures based on Ti_6Si_2B. For higher amounts, the Ti_5Si_3 or Ti_3Si phases dissolving alloying elements are preferentially formed instead the Ti_6Si_2B phase in the Ti-Si-B alloys containing alloying addition. Depending on milling time adopted, the Ti_6Si_2B phase was preferentially formed in microstructures of these quaternary alloys.

In this regard, the Ti alloys with cobalt addition are considered for biomedical applications due to their wear resistance and biocompatibility, which are produced by conventional melting and powder metallurgy techniques[6-10]. Porous Co-Ti alloys are prepared by powder metallurgy using the space holder technique[9]. $CoTi_2$ and α-Ti were identified in microstructure of Ti-4Co (wt.-%) alloy prepared by high-pressure torsion[11]. In contrast, the dense $TiC_xN_{(1-x)}$-15wt-%Co cermet materials were produced by mechanical alloying and subsequent spark plasma sintering, which presented an interesting combination of high hardness, fracture toughness and bending strength[12].

According to phase diagram of the Co-Ti system[13], the small Co amount lower than 1 and 15 at-% can dissolve at low and high temperatures in α-Ti and β-Ti, respectively. Larger Ti amounts close to 2 and 9 at-% are dissolved into

* e-mail: alfeu.ramos@unifal-mg.edu.br.

the Co lattices at low and high temperatures, respectively. The following intermediate phases are presents in this binary phase diagram: $CoTi_2$, CoTi, C15 (~66.6 at-%Co), C36 (~69 at-%Co) and Co_3Ti. CoTi exhibits a homogeneity range at low temperatures between 50 and 54 at-%Co. CoTi and $TiCo_2$ are formed by congruent transformations whereas the Ti_2Co, C15 and C36 occur by peritectic reactions.

No information was found in literature on effect of cobalt addition in phase transformations of Ti-Si-B alloys. In this sense, this work discusses on effect of cobalt doping and milling time on phase transformation of 65Ti-2Co-22Si-11B and Ti-6Co-22Si-11B (at-%) alloys produced by spark plasma sintering.

2. Experimental Procedure

In this work, the 65Ti-2Co-22Si-11B and 61Ti-6Co-22Si-11B (at-%) alloys were prepared by high-energy ball milling and subsequent spark plasma sintering (SPS). The following starting powders (Alfa Aesar, Ward Hill, MA, USA) were used to prepare these elemental powder mixtures: Ti (spherical, 99.9wt.-%), Si (irregular, 99.999wt.-%), and B (angular, 99.5 wt.-%). Cobalt granules with 99 wt.-% purity (Dinâmica Ltda., Indaiatuba, SP, Brazil) were used to prepare the quaternary alloys. In order to evaluate the effect of cobalt addition on the Ti_6Si_2B stability, the added amounts were chosen in accordance with previous works involving the Ti-Sn-Si-B[4] and Ti-Zr-Si-B[5] alloys produced by similar route with same alloying amounts.

Ball milling from elemental Ti-Co-Si-B powder mixtures was performed in a planetary Fritsch P-5 mill (Fritsch GmbH, Idar-Oberstein, Germany) under argon atmosphere using WC-6Co vials (225 mL) and balls (19 mm diameter), rotary speed of 300 rpm and a ball-to-powder weight ratio of 10:1. To understand the effect of milling time on phase transformation, the elemental Ti-Co-Si-B powder mixtures were milled at different times (20, 60, and 300 min), which are based on the previous work[4].

In the sequence, the Ti-Co-Si-B powders previously milled at different times were then consolidated by spark plasma sintering (SPS) in a Dr. Sinter – fdc SPS division model SPS-211LX sintering machine (FUJI Electron Industrial. Co. LTD) at 1100 °C for 12 min (minimum time to obtain high densification) under low vacuum (3.3×10^{-3} to 1×10^{-5} Pa) with a heating rate of 65 °C / min, using axial pressure of 20 MPa and a graphite die in order to obtain the cylinder specimens with 10 mm diameter. The temperature was measured by placing the radial pyrometer focused on the graphite die.

The as-milled Ti-Co-Si-B powders and the SPSed samples were evaluated by X-ray diffraction (XRD), scanning electron microscopy (SEM), energy dispersive spectrometry (EDS), laser diffraction particle size analysis. Furthermore, sintered samples were characterized by relative density using Arquimedes method and Vickers microhardness tests.

XRD experiments at room temperature of Ti-Co-Si-B samples were performed in a Panalytical model Empyrean equipment (PANalytical, Almelo, The Netherlands) using Cu-Kα radiation and a Ni filter, voltage of 40 kV, current of 30 mA, diffraction angle (2θ) in the range from 20 to 80º, angular pass of 0.02º and counting time per pass of 80s. The Pearson' crystal data[14] and the Powdercell computer program[15] were used to index the phases in XRD patterns of as-milled powders and SPSed samples. The values of lattice parameters, unit cell volume, and interplanar distance (d) of the α-Ti and bcc-Si peaks in Ti-Co-Si-B powder mixtures as well as their major diffraction angles (2θ) and relative phase amounts were calculated by Rietveld refining using the FullProf 2.7.9 program[16]. The crystallite sizes (D) of α-Ti and bcc-Si in as-milled Ti-Co-Si-B powders were calculated using the Scherrer equation[17,18].

SEM micrographs of as-milled Ti-Co-Si-B powders and their SPSed samples were obtained in a Hitachi model TM3000 SEM (Hitachi High-Technologies Corporation (TOKYO, Japan) using backscattered electron detector, whereas the Ti, Co and Si contents of phases formed in SPSed Ti-Co-Si-B samples were measured by EDS analysis using inner patterns. In SPSed Ti-Co-Si-B alloys, the samples were carefully prepared by conventional metallographic practices i.e., the sanding with SiC sandpapers (120, 200, 320, 400, 600 and 1200 #) and polishing with colloidal silica suspension. No chemical attack was needed for the microstructural characterization of these quaternary alloys. To identify the Ti, Si, B and Co distributions in microstructures of the SPSed 61Ti-6Co-22Si-11B alloy, the X-ray mapping was also conducted in SEM analysis.

The particle size distribution of as-milled Ti-Co-Si-B powders was performed by laser diffraction experiments in a Malvern Instruments model Mastersizer 2000 equipment (Malvern, Worcestershire, United Kingdom), using water as dispersant medium and Fraunhofer particle size. To measure the volume of fine particles, mean particle sizes and coarse particles in as-milled Ti-Co-Si-B powders, the values of D10, D50 and D90, which are the intercepts for 10%, 50% and 90% of the cumulative volume, respectively, were determined.

In order to correlate the microstructures and mechanical behavior of the SPSed Ti-Co-Si-B alloys, the values of Vickers microhardness were obtained in a Buehler model Micromet 6020 microhardness tester (Buehler, Lake Bluff, Illinois, USA) in accordance to the ASTM E-384 standard[19] using a load of 96 N under a loading rate of 0.01 mm/s. The average Vickers microhardness values were obtained in representative regions from ten measurements for each sample.

3. Results and Discussion

Figure 1 shows the XRD patterns of 65Ti-2Co-22Si-11B and 61Ti-6Co-22Si-11B powder mixtures at different milling times. Peaks of α-Ti, Si and Co were initially identified in powders milled for 20 min. Coherently, the Co peaks were more accentuated in Co-richer powder mixture. As expected, the relative intensity of peaks was promptly reduced for longer milling times due to severe plastic deformation and/or solid-state elemental dissolution during ball milling. Moreover, the Co peaks disappeared after milling for 60 and 300 min in 65Ti-2Co-22Si-11B and 61Ti-6Co-22Si-11B powders, respectively. Traces of Si and α-Ti peaks were identified in 65Ti-2Co-22Si-11B powders milled for 300 min, whereas only the peaks of Ti_5Si_3 and TiB were indexed in XRD patterns of 61Ti-6Co-22Si-11B powders milled for 300 min only. It was noted that the α-Ti peaks were slightly moved in the direction of larger diffraction angles (2θ), suggesting

that Si, B and/or Co atoms were dissolved into its crystalline structure to form supersaturated solid solutions. According to the phase diagram of the Co-Ti[13], B-Ti[20] and Si-Ti[21] systems, the α-Ti can dissolve the cobalt (or boron) and silicon amounts lower than 1 and 2 at-%, respectively. However, no intermediate intermetallic phase based on the Co-Ti, Co-B or Co-Si system was formed during ball milling from the elemental Ti-Co-Si-B powder mixtures.

The relative phase amounts in 65Ti-2Co-22Si-11B and 61Ti-6Co-22Si-11B powders are presented in Table 1, which were determined by Rietveld refining. Independently on powder composition, the amounts of α-Ti were continuously increased whereas the amounts of Si were reduced during ball milling of these powder mixtures. Cobalt was not measured due to its relatively small amounts in these powder mixtures.

Table 2 shows the values of lattice parameters and unit cell volume of α-Ti and bcc-Si in Ti-Co-Si-B powders milled at different times, which were determined by Rietveld refining. Titanium, cobalt, silicon and boron possesses atomic radium (covalent radium) of 140 (136) pm, 126 (152) pm, 111 (111) pm and 87 (82) pm, respectively. Initially, the α-Ti presents the *a* and *c* lattice parameters of 0.29616 and 0.47589 nm, respectively with unit cell volume of 0.0361 nm^3. Our results have indicated that these values were slightly reduced during ball milling of 65Ti-2Co-22Si-11B and 61Ti-6Co-22Si-11B powders which could be related to the elemental dissolution into the α-Ti lattice. However, it was not noted any significant change in these values for the Co-richer powders and longer milling times. Bcc-Si presents the lattice parameters and unit cell volume of 0.543 nm and 0.1601 nm^3, respectively. Independently on powder composition and milling time, no significant change in these values was achieved.

Values of interplanar distance (d), crystallite size (D) and major α-Ti and bcc-Si diffraction angles (2θ) in 65Ti-2Co-22Si-11B and 61Ti-6Co-22Si-11B powders milled at different times are presented in Table 3, which were determined by Rietveld refining. Excepting to the 65Ti-2Co-22Si-11B powders milled for 20 min, the major α−Ti peak was broadened and moved in the direction of larger diffraction angles (2θ) after milling for 60 and 300 min. These facts are normally related to the crystallographic distortions due to severe plastic deformation and atomic dissolution occurred during milling[22], suggesting that the powder mixture with lesser cobalt amounts presented superior plastic deformation. However, the released heat from exothermic and partial Ti_5Si_3 formation has reduced the metastability of supersaturated

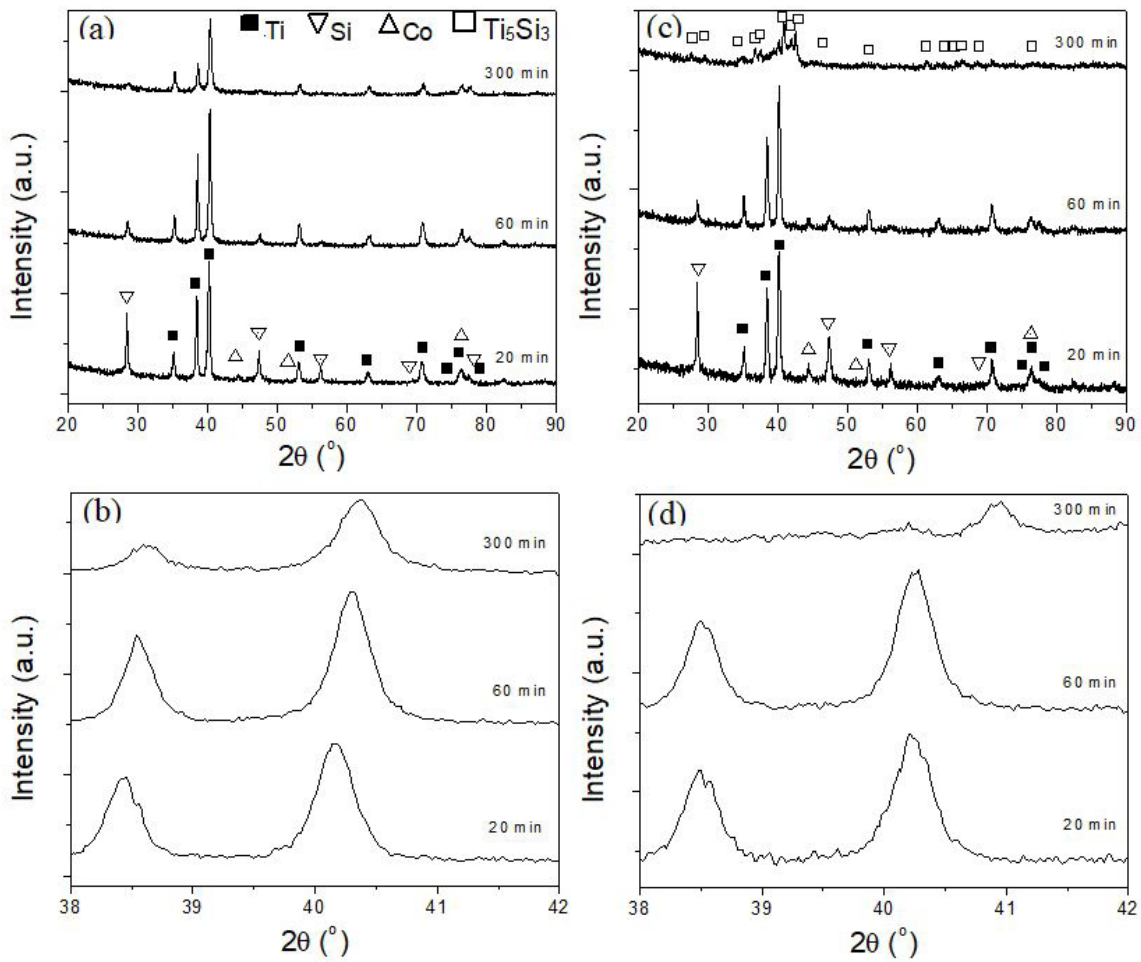

Figure 1. XRD patterns of (a,b) Ti-2Co-22Si-11B and (c,d) Ti-6Co-22Si-11B powder mixtures at different milling times, and their details on their major α-Ti peaks are illustrated in (b) and (d), respectively.

Table 1. Relative phase amounts determined by Rietveld refining in 65Ti-2Co-22Si-11B and 61Ti-6Co-22Si-11B powders milled at different times.

Milling Time (min)	65Ti-2Co-22Si-11B			61Ti-6Co-22Si-11B		
	α-Ti	Si	Co	α-Ti	Si	Co
20	63.6	36.4	---	69.6	30.4	---
60	82.2	17.6	---	80.8	19.2	---
300	93.4	6.1	---	---	---	---

Table 2. Lattice parameters and unit cell volume of α-Ti and bcc-Si determined by Rietveld refining of Ti-Co-Si-B powders milled at different times.

Milling Time (min)	65Ti-2Co-22Si-11B				61Ti-6Co-22Si-11B			
	α-Ti, Lattice Parameters (nm)			α-Ti, Cell Volume (nm^3)	α-Ti, Lattice Parameters (nm)			α-Ti, Cell Volume (nm^3)
20	0.2950	0.2950	0.4679	0.03527	0.2951	0.2951	0.4681	0.03532
60	0.2951	0.2951	0.4683	0.03533	0.295	0.2950	0.4683	0.03531
300	0.2948	0.2948	0.4678	0.03521	ND	ND	ND	ND
	Si, Lattice Parameters (nm)			Si, Cell Volume (nm^3)	Si, Lattice Parameters (nm)			Si, Cell Volume (nm^3)
20	0.5427	0.5427	0.5427	0.15985	0.5429	0.5429	0.5429	0.16004
60	0.5434	0.5434	0.5434	0.16046	0.5429	0.5429	0.5429	0.16007
300	0.5421	0.5421	0.5421	0.15931	ND	ND	ND	ND

ND - Not Determined.

Table 3. Interplanar distance (d), crystallite size (D), diffraction angle (2θ) of major α-Ti and bcc-Si peaks in 65Ti-2Co-22Si-11B and 61Ti-6Co-22Si-11B powders milled at different times, which were determined by Rietveld refining.

Milling Time (min)	α-Ti in 65Ti-2Co-22Si-11B			bcc-Si in 65Ti-2Co-22Si-11B		
	Interplanar distance, d (nm)	Crystallite size, D (nm)	2θ, (°)	Interplanar distance, d (nm)	Crystallite size, D (nm)	2θ, (°)
20	0.22451	24.2	40.133	0.31388	34.8	28.421
60	0.22378	24.8	40.267	0.31267	18.8	28.521
300	0.22347	18.6	40.325	0.31206	9.8	28.580
Milling Time (min)	α-Ti in 61Ti-6Co-22Si-11B			bcc-Si in 61Ti-6Co-22Si-11B		
	Interplanar distance, d (nm)	Crystallite size, D (nm)	2θ, (°)	Interplanar distance, d (nm)	Crystallite size, D (nm)	2θ, (°)
20	0.22413	22.80	40.202	0.31311	33.3	28.484
60	0.22404	24.58	40.219	0.31298	21.4	28.495
300	ND	ND	ND	ND	ND	ND

ND - Not Determined.

Ti solid solution in powder mixtures with 6 at-% Co. Peaks of Ti_5Si_3 were also identified in 61Ti-6Co-22Si-11B powders milled for 300 min. Hence, the FWHM values and diffraction angles of major α-Ti peak were not determined, which are indicated in Table 3 as ND (Not Determined).

Figure 2 displays the SEM micrographs of the 65Ti-2Co-22Si-11B and 61Ti-6Co-22Si-11B powder mixtures at different milling times. As expected for these powder mixtures containing both ductile and brittle components, the brittle Si and B particles were promptly fragmentated whereas the ductile Ti and Co particles suffered severe plastic deformation provided by the impact and shear mechanisms during ball milling. As consequence of large amounts of ductile components, the powder particles or aggregate sizes with rounded morphologies increased during milling up to 60 min, which were subsequently reduced in powders milled for 300 min. This fact was more pronounced in the Co-richer powder mixture due to the *in-situ* formation of hard and brittle Ti_5Si_3 compound.

Values of D10, D50 and D90 as well as the specific surface area measured by laser diffraction experiments in as-milled Ti-Co-Si-B powders are presented in Table 4, whereas their particle size distribution curves are illustrated in Figure 3. According with the SEM observations, the average particle sizes (D50) were continuously increased during milling for 300 min of the 65Ti-2Co-22Si-11B and 61Ti-6Co-22Si-11B powders, respectively. Excepting in 61Ti-6Co-22Si-11B powders milled for 300 min, the average particle sizes were reduced to 88 μm owing mainly the in-situ Ti_5Si_3 formation. Bimodal curves of Ti-Co-Si-B powders milled for 20 min with a slight normal region for finer particles can be also observed in Figure 3. The 65Ti-2Co-22Si-11B powders milled for 60 and 300 min exhibited unimodal distribution curves. Despite the smaller average particle sizes, the 61Ti-6Co-22Si-11B powders milled for 300 min presented a bimodal distribution, indicating the significant existence of coarse particles/aggregates. In this way, the values of specific surface area were reduced from 0.32/0.34 to 0.042/0.12 m^2/g in the

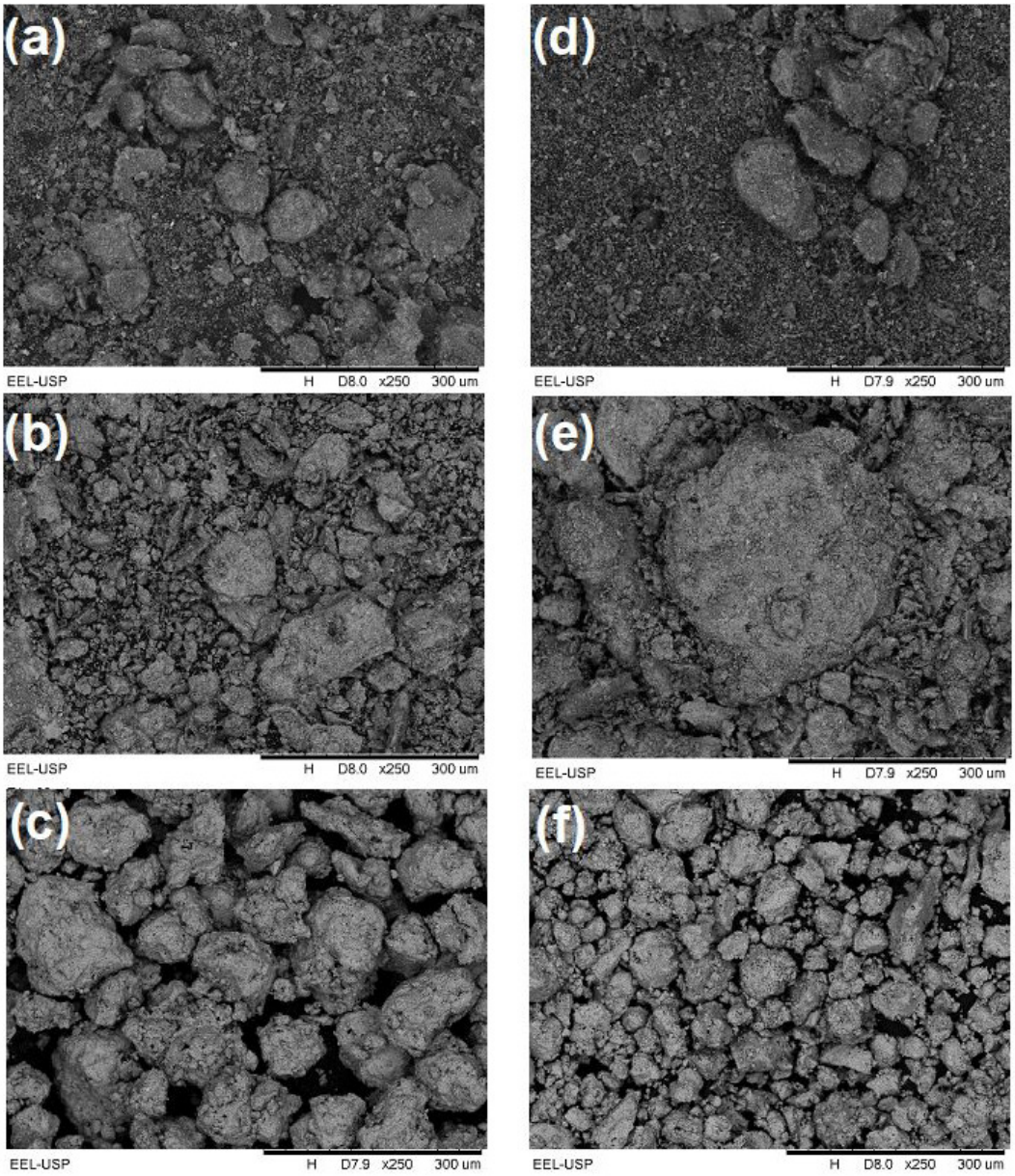

Figure 2. SEM micrographs of the (a-c) Ti-2Co-22Si-11B and (d-f) Ti-6Co-22Si-11B powder mixtures at different milling times: (a,d) 20 min, (b,e) 60 min, and (c,f) 300 min.

Table 4. Values of D10, D50 and D90 as well as the specific surface area measured by laser diffraction experiments in as-milled Ti-Co-Si-B powders.

Composition Alloy (at.-%)	Milling Time (min)	D10 (μm)	D50 (μm)	D90 (μm)	Specific Surface Area (m^2/g)
65Ti-2Co-22Si-11B	20	11.68	94.04	216.37	0.32
	60	25.05	119.50	391.07	0.17
	300	77.95	208.35	452.26	0.042
61Ti-6Co-22Si-11B	20	11.36	101.59	227.17	0.34
	60	24.97	115.53	403.11	0.16
	300	26.51	88.81	473.68	0.12

65Ti-2Co-22Si-11B / 61Ti-6Co-22Si-11B powder mixtures, as are illustrated in Figure 3.

XRD patterns of the SPSed 65Ti-2Co-22Si-11B and 61Ti-6Co-22Si-11B alloys previously milled at different times are presented in Figure 4. Results have indicated the presence of intense Ti_5Si_3, TiB and Ti_6Si_2B peaks. It was noted that the relative intensity of Ti_6Si_2B was reduced whereas that to the Ti_5Si_3 phase increased with the cobalt amount

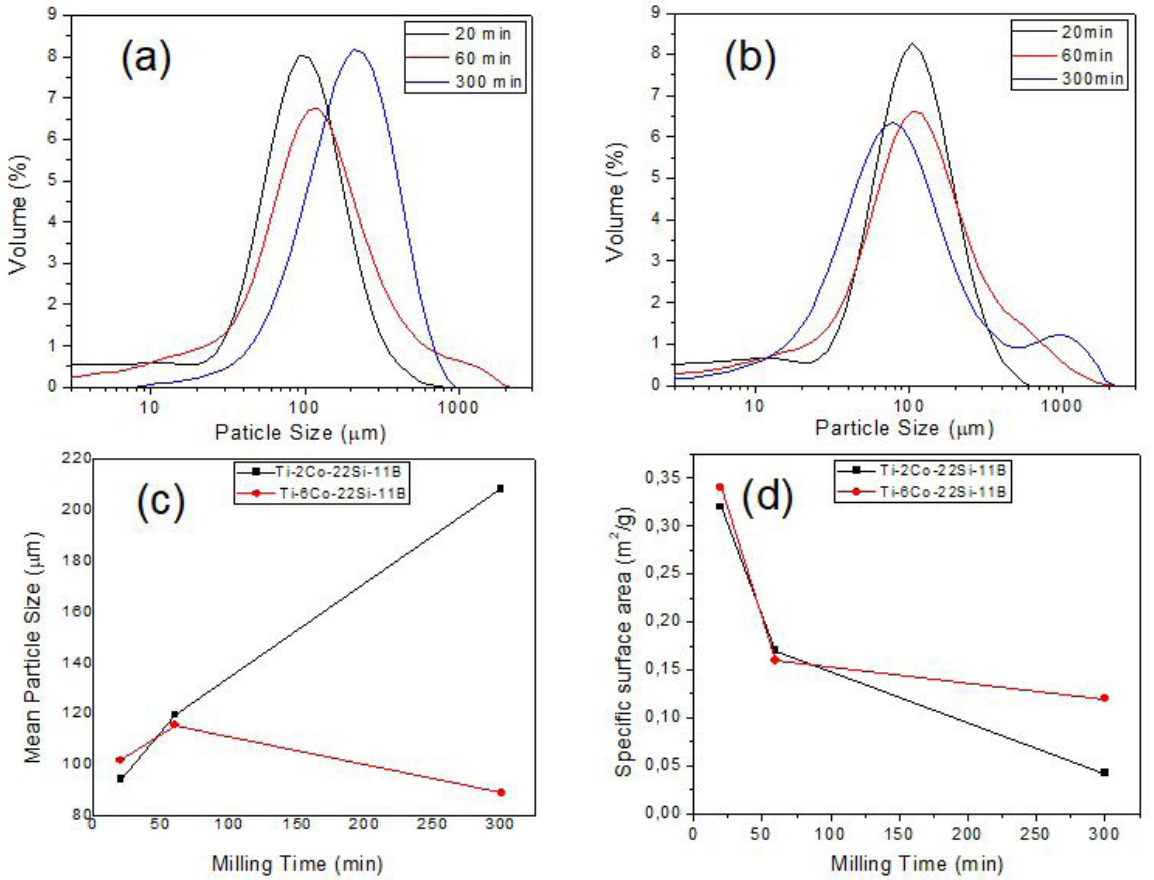

Figure 3. Particle size distribution curves of the (a) Ti-2Co-22Si-11B and (b) Ti-6Co-22Si-11B powder mixtures after different milling times. In (c) and (d), the effect of composition and milling time on the average particle sizes and specific surface areas of the Ti-Co-Si-B powders, respectively.

increased in the nominal alloy composition. Consequently, a larger amount of TiB is formed in microstructure of the SPSed 61Ti-6Co-22Si-11B alloy and its peaks more intense can be achieved. CoTi was also indexed in XRD patterns of the SPSed 61Ti-6Co-22Si-11B alloy produced with powders previously milled for 60 and 300 min. Independent on adopted milling time, the minor TiC peaks were also identified in XRD patterns of these quaternary alloy, indicating that the carbon contamination was provided during spark plasma sintering.

Figure 5 shows the representative X-ray mapping of the 61Ti-6Co-22Si-11B alloy which it was produced with powders milled for 300 min. Results have revealed that the brighter regions in microstructure of this quaternary alloy are the richer Co sites, whereas its matrix contains the richer regions of Si and B, i.e., probably the Ti_6Si_2B and Ti_5Si_3 phases. In this way, titanium was uniformly distributed in both the matrix and others intermetallic precipitates. Boron was identified in dark regions with acicular morphology.

SEM micrographs of the (a-c) SPSed 65Ti-2Co-22Si-11B and (d-f) 61Ti-6Co-22Si-11B alloys produced with powders previously milled for, 20, 60 and 300 min are presented in Figure 6. The microstructures of these alloys presented very small amounts of pores, indicating that the parameters used in SPS process were effectives to obtain dense materials. In general, all the sintered samples showed high relative density, greater than 97 ± 2%, inferring that the SPS process has allowed the densification of the samples at 1100 °C - 12 min / 20 MPa.

Despite the short milling (20 min) and sintering (12 min) times adopted for processing of these quaternary alloys, the atomic diffusion happened and the binary and ternary phases were formed in their microstructures. α-Ti, Ti_6Si_2B (matrix), Ti_5Si_3 and TiB were formed in microstructures of the SPSed 65Ti-2Co-22Si-11B alloy produced with powders milled for 20 and 60 min. It was also noted the presence of Co-rich precipitates located in brighter regions of the SPSed 65Ti-2Co-22Si-11B alloy produced with powders milled for 300 min. Independent on milling time, it was identified the existence of cracks in some regions of the SPSed 61Ti-6Co-22Si-11B alloy, which are related to the Ti_5Si_3 phase with high crystallographic anisotropy in accordance with previous works[6-9]. The microstructure of the SPSed 61Ti-6Co-22Si-11B alloy produced with powders milled for 20 min has indicated the major Ti_5Si_3 presence beside the α-Ti, TiB and Ti_6Si_2B precipitates. Nonetheless, the Co-rich phases in brighter regions were also observed in microstructures of the 61Ti-6Co-22Si-11B alloy produced with powders milled for 60 and 300 min only.

EDS results showing the typical Ti, Co and Si contents of phases formed in microstructures of the SPSed 65Ti-

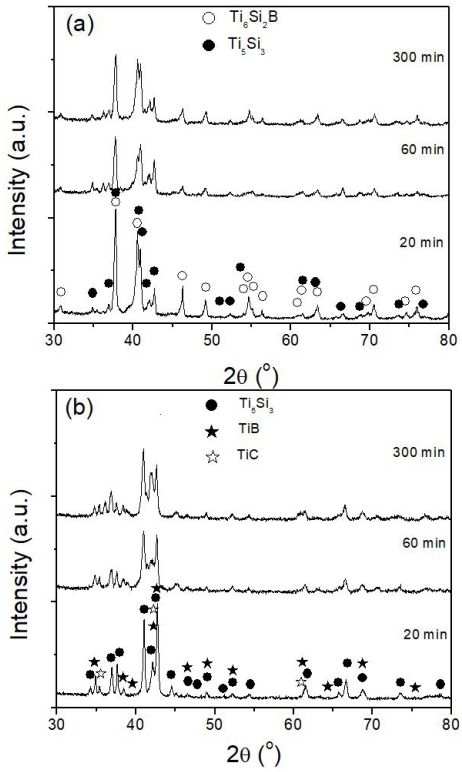

Figure 4. XRD patterns of the spark plasma sintered (a) Ti-2Co-22Si-11B and (b) Ti-6Co-22Si-11B alloys produced with powders previously milled for 20 min, 60 min and 300 min.

2Co-22Si-11B and 61Ti-6Co-22Si-11B alloys produced with powders milled at different times are presented in Table 5. Values with asterisk were measured in alloys produced from the powders milled for 300 min. In SPSed 65Ti-2Co-22Si-11B alloy, the α-Ti regions have presented the Si and Co contents between 1.7-3.7 and 0.3-3.3 at-%, respectively. TiB has dissolved 1.7-5.7 at-% Si and 0-0.2 at-% Co, whereas the ternary Ti_6Si_2B phase exhibited 20.1-27.5 at-% Si and 0.1-2.7 at-% Co. It is interesting to note that the Ti_5Si_3 has dissolved smaller amounts of Co (<0.8 at-%) than the Ti_6Si_2B phase. Moreover, the highest Co amounts in Ti_6Si_2B and Ti_5Si_3 were measured in SPSed 65Ti-2Co-22Si-11B alloy produced from the powders milled for 300 min. As expected, the better chemical uniformity and smaller diffusion paths needed to atomic dissolution has happened in powder particles for longer milling times. Others brighter regions containing 4.6-8 and 16.7-20.6 at-% Co were also detected in microstructures of 65Ti-2Co-22Si-11B alloys produced with powders milled for 20 (and 60) and 300 min, respectively. Independent on the milling time, the nominal alloy composition of this quaternary SPSed alloy was confirmed by EDS results, which had the Si and Co contents close to 22.8-26.4 and 1.7-1.9 at-%, respectively.

Ti_6Si_2B presented 17.2 at-% Si and 0.5 at-% Co in microstructure of the SPSed 61Ti-6Co-22Si-11B alloy produced with powders milled for 20 min. Ti_6Si_2B was not identified in microstructures of this quaternary alloy produced with powders milled for 60 and 300 min. In microstructures of this alloy produced with powders milled

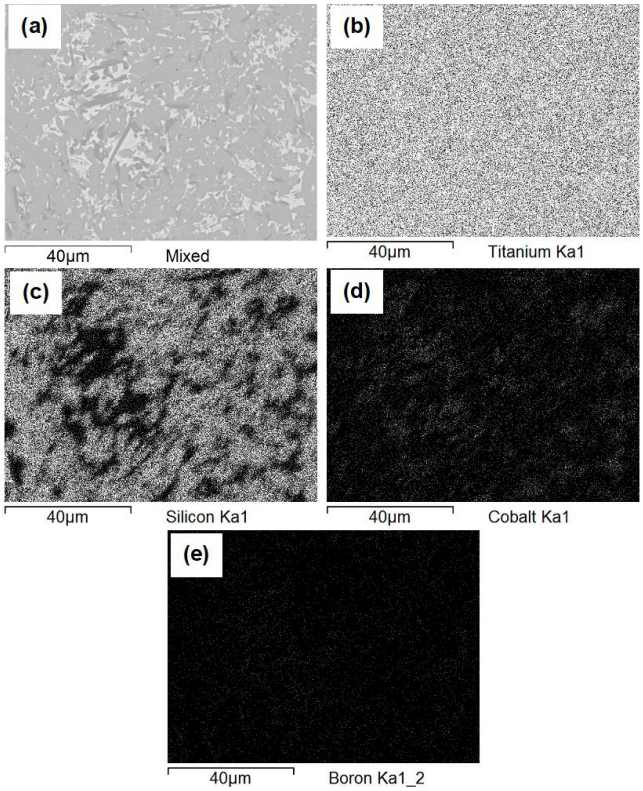

Figure 5. X-ray mapping of the SPSed Ti-6Co-22Si-11B alloy produced with powders milled for 300 min, showing the elemental distribution in its microstructure: (a) pattern, (b) titanium, (c) silicon, (d) cobalt, and (e) boron.

for 20 (and 60) and 300 min, the Ti_5Si_3 phase presented the Si contents varying between 35.5-36.8 and 30.6-35.7 at-%, whereas the Co contents were in the range of 1.3-1.7 and 1.9-4.2 at-%, respectively. TiB dissolving up to 5.5 at-% Si and 2.7 at-% Co were measured in microstructures of these quaternary alloy produced with powders milled for 300 min. Our results have indicated that a more pronounced Co dissolution in Ti_5Si_3 and TiB was favored with increasing the Co amount in starting powders milled at longer times. Moreover, the CoTi phase was' identified in brighter regions of these quaternary alloy produced with powders milled for 20 and 60 min, which presented the Si and Co contents in the range of 4.6-4.7 and 41.3-43.0 at-%, respectively. Moreover, it was noted the presence of others bright regions containing 4.4-16.7 at-% Si and 15.6-26.2 at-% Co in this quaternary alloy produced with powders milled for 300 min, which are related to the $CoTi_2$ phase. However, an unknown phase containing close to 25 at-% Co (dissolving some Si amount) was found in microstructures of the SPSed 65Ti-2Co-22Si-11B (300 min) and 61Ti-6Co-22Si-11B (60 and 300 min) alloys, suggesting to be the $CoTi_3$ phase. However, this binary phase is not reported in the phase diagram of the Co-Ti system[13]. Despite the presence of TiC peaks in XRD pattern of SPSed 61Ti-6Co-22Si-11B alloy no evidence was found in EDS analysis by SEM.

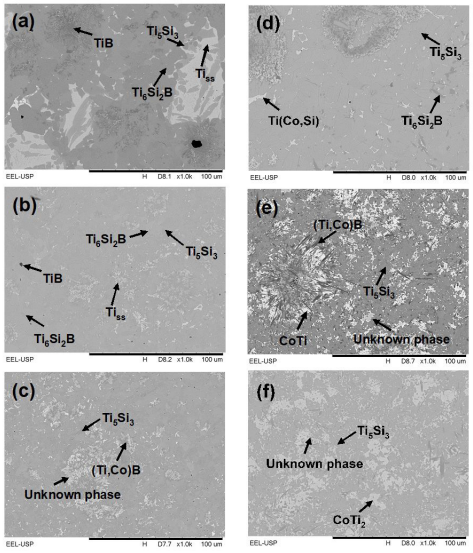

Figure 6. SEM micrographs of the SPSed (a-c) Ti-2Co-22Si-11B and (d-f) Ti-6Co-22Si-11B alloys produced with p'owders milled at different times: (a,d) 20 min, (b,e) 60 min, and (c,f) 300 min.

The Vickers microhardness values of the SPSed 65Ti-2Co-22Si-11B and 61Ti-6Co-22Si-11B alloys produced with powders milled at different times are presented in Figure 7. Independent on the milling time, it was also noted that the Co-richer alloy exhibited the highest Vickers microhardness values, which can be related to the Co-rich intermetallic phases. The 65Ti-2Co-22Si-11B and 61Ti-6Co-22Si-11B alloys presented the values between 950-1050 HV and 1050-1150 HV, respectively. In contrary, the SPSed Ti-2Zn-22Si-11B alloy presented average Vickers hardness values higher than 1050 HV whereas the SPSed Ti-6Zn-22Si-11B alloy varied between 970 and 1036 HV, which were associated with the Ti_6Si_2B formation[4]. Considering the SPSed Ti-Co-22Si-11B and Ti-2Sn-22Si-11B alloys are based on Ti_6Si_2B as matrix, and both the Co and Tin solubility limits in Ti_6Si_2B are closed to 2 at-%, their Vickers microhardness values of these quaternary alloys can be related with a more effective $(Ti,Sn)_6Si_2B$ solution strengthening.

Nonetheless, the Ti-28Nb-7Ta-5Zr-10Hap alloy produced by mechanical alloying and spark plasma sintering has exhibited microhardness close to 537 HV[23]. The Vickers

Table 5. Typical Ti, Si and Co (at.-%) contents measured by EDS analysis in phases formed of the SPSed 65Ti-2Co-22Si-11B and 61Ti-6Co-22Si-11B alloys produced with powders milled for 20 and 300 min.

65Ti-2Co-22Si-11B			
Phase	**Ti (%-at.)**	**Si (%-at.)**	**Co (%-at.)**
Ti	98.0 – 93.0	1.7 – 3.7	0.3 – 3.3
Ti_6Si_2B	77.1* – 72.2	20.1* – 27.5	0.1 – 1.7/2.7*
Ti_5Si_3	63.0* – 68.0	31.4 – 36.2*	0.6 – 0.8*
TiB	98.2 – 94.3	1.7 – 5.7	0.2 – 0
ND	89.2 – 89.8	2.8 – 5.5	8.0 – 4.6
ND	81.7* – 77.4*	1.6* – 2.0*	16.7* – 20.6*
Global	71.7* – 75.5	22.8 – 26.4*	1.7 – 1.9*
61Ti-6Co-22Si-11B			
Phase	**Ti (at.-%)**	**Si (at.-%)**	**Co (at.-%)**
Ti_6Si_2B	82.3 – 77.8	17.2 – 23.2	0 – 0.5
Ti_5Si_3	61.4 – 63.2	36.8 – 35.5	1.7 – 1.3
CoTi	52.3 – 54.1	4.7 – 4.6	43.0 – 41.3
Global	65.6 – 65.7	29.3 – 29.2	5.1 – 5.0
***TiB**	97.8 – 91.8	1.1 – 5.5	1.2 – 2.7
***Ti_5Si_3**	62.9 – 65.2	35.7 – 30.6	1.9 – 4.2
***ND**	74.9 – 78.5	2.1 – 2.1	23.1 – 19.4
***$CoTi_2$**	69.5 – 67.7	4.4 – 16.7	26.2 – 15.6

ND - Not Determined; * measured in alloy produced with powders milled for 300 min.

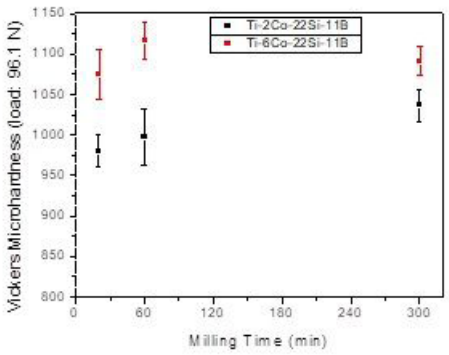

Figure 7. Vickers Hardness values of the SPSed (a-c) Ti-2Co-22Si-11B and (d-f) Ti-6Co-22Si-11B alloys produced with powders milled at different times: (a,d) 20 min, (b,e) 60 min, and (c,f) 300 min.

hardness values of homogenized Ti-48Al-2Cr and Ti-48Al-2Cr-2Nb alloys varied from 274 and 542 to 303 and 610 HV, respectively[24]. In these alloys, the higher hardness in the quaternary alloy is due to the presence of larger amounts of lamellar phase as compared to ternary alloy where the amount of γ phase rich regions is found to be greater. However, the mechanically alloyed and spark plasma sintered Ti-Co-Si-B alloys evaluated in this work have presented higher Vickers hardness than others alloys used to biomedical, automotive and aerospace applications.

4. Conclusions

Longer milling times (300 min) contributed to reach the chemical and microstructural homogeneities in the 65Ti-2Co-22Si-11B and 61Ti-6Co-22Si-11B powder mixtures, and supersaturated α-Ti solid solutions were achieved.

Spark plasma sintering produced dense 65Ti-2Co-22Si-11B and 61Ti-6Co-22Si-11B alloys. Despite the short sintering time (12 min), the equilibrium microstructures were reached using powders milled for longer times.

The increase of Co in the nominal alloy composition has reduced the Ti_6Si_2B amount in microstructures of the SPSed Ti-Co-Si-B alloys, and others Co-rich phases were preferentially formed.

Vickers hardness values of the SPSed 65Ti-2Co-22Si-11B and 61Ti-6Co-22Si-11B alloys were close to 950-1050 HV and 1050-1150 HV, respectively.

5. Acknowledgments

Authors thank to FAPESP (grants #2001/03961-4 and #2007/50018-2)-, CAPES-, FAPEMIG-, CNPq (grant #313052/2019-7)- and FINEP-Brazil for the financial supports needed in development of this work.

6. References

1. Kato MKN, Onari E, Arisawa EAL, Silva NS, Ramos AS. Osseointegration features of orthopedic Ti-10Si-5B implants. Mater Sci Eng C. 2009;29(3):980-6. http://dx.doi.org/10.1016/j.msec.2008.08.022.
2. Fernandes BB, Ueda M, Savonov GS, Moura C No, Ramos AS. Surface corrosion of Ti-16Si-4B powder alloy implanted with nitrogen by plasma-based technique. IEEE Transactions on Plasma Science. 2011;39(11):3061-66. https://doi.org/10.1109/TPS.2011.2159031.
3. Samarov V, Seliverstov D, Froes FH (Sam). 18 - Fabrication of near-net-shape cost-effective titanium components by use of prealloyed powders and hot isostatic pressing. Qian M Froes FH (Sam), editors. Titanium powder metallurgy: science, technology and applications. Oxônia: Butterworth-Heinemann; 2015. p. 313-6. https://doi.org/10.1016/B978-0-12-800054-0.00018-6.
4. Ferreira ND, Leal RM No, Filgueira M, Ferreira LM, Alves MFRP, Ramos ECT, et al. Microstructure and Vickers hardness of mechanically alloyed and spark plasma sintered Ti-2Zn-22Si-11B and Ti-6Zn-22Si-11B alloys. J Alloys Compd. 2019;794:615-24. http://dx.doi.org/10.1016/j.jallcom.2019.04.172.
5. Rossi LB, Ferreira LM, Freitas BX, Nunes CA, Ramos AS, Filgueira M, et al. Mechanical alloying and hot pressing of Ti-Zr-Si-B powder mixtures. Metals (Basel). 2018;8:82-94. http://dx.doi.org/10.3390/met8020082.
6. Matković T, Slokar L, Matković P. Structure and properties of biomedical Co–Cr–Ti alloys. J Alloys Compd. 2006;407(1-2):294-8. http://dx.doi.org/10.1016/j.jallcom.2005.06.025.
7. Weng W, Biesiekierski A, Li Y, Wen C. Effects of selected metallic and interstitial elements on the microstructure and mechanical properties of beta titanium alloys for orthopedic applications. Materialia. 2019;6:100323. http://dx.doi.org/10.1016/j.mtla.2019.100323.
8. Niinomi M. 4.1 - Titanium spinal-fixation implants. In Froes FH, Qian M, editors. Titanium in medical and dental applications. Cambridge: Woodhead Publishing; 2018. p. 347-69 (Woodhead Publishing Series in Biomaterials). http://dx.doi.org/10.1016/B978-0-12-812456-7.00016-0.
9. Mutlu I. Synthesis and characterization of Ti–Co alloy foam for biomedical applications. Trans Nonferrous Met Soc China. 2016;26(1):126-37. http://dx.doi.org/10.1016/S1003-6326(15)64028-6.
10. Xue Y, Wang HM. Microstructure and dry sliding wear resistance of CoTi intermetallic alloy. Intermetallics. 2009;17(3):89-97. http://dx.doi.org/10.1016/j.intermet.2008.06.010.
11. Straumal BB, Kilmametov AR, Ivanisenko Y, Mazilkin AA, Hahn H. Diffusive and displacive phase transitions in Ti–Fe and Ti-Co alloys under high-pressure torsion. J Alloys Compd. 2018;735:2281-6. http://dx.doi.org/10.1016/j.jallcom.2017.11.317.
12. Borrell A, Salvador MD, Rocha VG, Fernández A, Gotor FJ. Bulk TiCxN1−x–15%Co cermets obtained by direct spark plasma sintering of mechanochemical synthesized powders. Mater Res Bull. 2012;47(12):4487-90. http://dx.doi.org/10.1016/j.materresbull.2012.09.066.
13. Murray JL. The Co-Ti (Cobalt-Titanium) system. In: Okamoto H., Schlesinger ME, Mueller E.M., editors. Binary alloy phase diagrams. Vol. 3. New York: ASM International; 2016. p. 674-5. https://doi.org/10.31399/asm.hb.v03.9781627081634.
14. Villars P, Cenzual K. Pearson's crystal data: crystal structure database for inorganic compounds (on DVD), release 2018/19. Materials Park: ASM International.
15. Kraus W, Nolze G. Powdercell: a program for the representation and manipulation of crystal structures and calculation of the resulting X-ray powder patterns. J Appl Cryst. 1996;29:301-3. http://dx.doi.org/10.1107/S0021889895014920.
16. Rietveld HM. A profile refinement method for nuclear and magnetic structures. J Appl Cryst. 1969;2:65-71. http://dx.doi.org/10.1107/S0021889869006558.
17. Scherrer P. Bestimmung der Größe und der inneren Struktur von Kolloidteilchen mittels Röntgenstrahlen. Nachrichten von der Gesellschaft der Wissenschaften zu Göttingen, Abh. Math.-Phys. Kl. [serial on the Internet]. 1918 [cited 2020 Jul 22];2:98-100. Available from: http://www.digizeitschriften.de/dms/resolveppn/?PID=GDZPPN002505045

18. Patterson AL. The scherrer formula for X-ray particle size determination. Phys Rev. 1939;56(10):978-82. http://dx.doi.org/10.1103/PhysRev.56.978.
19. ASTM International. ASTM E384-17: Standard Test Method for Microindentation Hardness of Materials. West Conshohocken: ASTM; 2017.
20. Predel B. B - Ti (Boron - Titanium). In: Landolt-Börnstein - Group IV Physical Chemistry, B-Ba – Cu-Zr. USA: Springer-Verlag Berlin Heidelberg; 2012. https:// dx.doi.org/10.1007/978-3-540-44756-6_41.
21. Fiore M, Beneduce F No, Azevedo CRF. Assessment of the Ti-Rich corner of the Ti-Si phase diagram: the recent dispute about the eutectoid reaction. Mater Res. 2016;19(4):942-53. http://dx.doi.org/10.1590/1980-5373-MR-2016-0157.
22. Suryanarayana C. Mechanical alloying and milling. Prog Mater Sci. 2001;46(1-2):1-184. http://dx.doi.org/10.1016/S0079-6425(99)00010-9.
23. Bhushan B, Singh A, Singh R, Mehta JS, Prakash C. Fabrication and characterization of a new range of β-type Ti-Nb-Ta-Zr-xHaP (x=0, 10) alloy by mechanical alloying and spark plasma sintering for biomedical applications. Mater Today. 2018;5(14):27749-56. http://dx.doi.org/10.1016/j.matpr.2018.10.010.
24. Gupta RK, Pant B, Agarwala V, Agarwala RC, Sinha PP. Evaluation of Ti aluminide intermetallics processed through reaction synthesis. High-Temp Mater Process. 2009;28(3):121-32. http://dx.doi.org/10.1515/HTMP.2009.28.3.121.